Available online at www.sciencedirect.com
SCIENCE DIRECT®
International Journal of Heat and Fluid Flow 25 (2004) 32–43
International Journal of HEAT AND FLUID FLOW
www.elsevier.com/locate/ijhff

Simulations of laminar and transitional cold wall jets

Pratik Bhattacharjee, Eric Loth *

Department of Aeronautical and Astronautical Engineering, University of Illinois Urbana Champaign, 104 S Wright St., Urbana, IL 61801, USA

Received 6 March 2003; accepted 4 November 2003

Abstract

The wall jet studied herein is a fundamental idealization of a refrigerated air curtain. Specifically, two-dimensional and three-dimensional idealized cold wall-jets are studied at a variety of flow conditions (different inflow profiles and Reynolds numbers) to investigate the effect on wall jet thickness and temperature distributions. The objective of the work is to allow an increased understanding of the evolution of temperature distribution within wall jets for laminar and transitional flow conditions, and the corresponding jet thicknesses. The primary simulation technique is direct numerical simulation (DNS) of the full Navier–Stokes equations, possible at modest Reynolds numbers. However, at higher Reynolds numbers a conventional Reynolds-averaged Navier–Stokes approach is also employed. Significant variations in wall jet thickness (both in terms of time-dependent variations and the time-averaged mean) are found as a function of Reynolds number, with a minimum occurring at flow speeds immediately prior to transition. The wall jet evolution (in terms of temperature distribution and jet thickness) is also sensitive to the inflow; whereby a constant gradient profile provides the lowest growth rates. Interestingly, the Reynolds-averaged Navier–Stokes approach yields quantitatively similar results to the 2-D and 3-D DNS approach at a wall-jet Reynolds number of 2000.

Keywords: Laminar; Wall-jet; Refrigeration; Transition

1. Introduction

1.1. Motivation

To maintain the interior at a low temperature while allowing open access, refrigerated display-cases rely on an air curtain to contain and deliver cold air to the product within the case. The overall fluid dynamics of the air curtain are quite complex and not well understood, but are important because they control the entrainment. Entrainment of ambient air into the air curtain increases the heat flux across the curtain and thus the load on the refrigeration unit in the case which, in turn, is directly related to the overall thermal efficiency of the unit. As such, the entrainment should be ideally minimized to reduce the energy requirements. The ideal velocity profile for minimum entrainment is suspected (based on internal qualitative studies by manufacturers) to have higher velocities near the inner portion. But, as discussed by Field and Loth (2001), there have been no studies in the open literature which have quantitatively examined the sensitivity of momentum or thermal entrainment to various velocity profiles. Several researchers have attempted predictions of the air-curtains using RANS (Reynolds-averaged Navier–Stokes) techniques, but with only qualitative success (Navaz et al., 2002; Baleo et al., 1995; George and Buttsworth, 2000). In addition, the influence of Reynolds number is not well understood especially near the regime of laminar and early transitional flow.

For a more fundamental description for the physics of the air curtain, the complex and case-specific geometries for a fully stocked case can be reasonably simplified to that of a wall jet with no initial turbulence. This is also consistent with the type of changes which may help reduce turbulent entrainment. This approximation is supported by recent experimental work by Field (2001), which has shown that the wall jet (with small Richardson number, i.e. negligible buoyancy effects) is a reasonable first approximation of the fluid physics observed in a refrigerated air curtain for a fully-stocked display-case.

* Corresponding author. Tel.: +1-217-244-5581; fax: +1-217-244-0720.
E-mail address: e-loth@uiuc.edu (E. Loth).

0142-727X/$ - see front matter © 2003 Published by Elsevier Inc.
doi:10.1016/j.ijheatfluidflow.2003.11.001

1.2. Previous wall jet studies

Since the early work of Glauert (1956), several experiments have been conducted to describe the flow structure of laminar and turbulent wall jets. However, few investigations have been focused on transitional wall jets. The studies that do involve the transitional nature have focused on understanding the dominating factors influencing the initiation of turbulence, and have been typically experimental in nature.

Hsiao and Sheu (1996) studied the flow transition in a plane wall jet using hot-wire anemometry for Reynolds numbers ranging from 300 to 30,000. Their results indicated that the wall-jet transition is initially triggered by the primary shear layer vortex and that the transition process strongly depends on the Reynolds number of the nozzle exit. It was seen that the unsteadiness and downstream turbulence began at approximately $Re = 750$. The finding of an increase in unsteadiness with Reynolds number is attributed to the successively earlier initiation of turbulence and also leads to increased wall jet thickness.

Recent experimental work on transitional wall jet flows by Gogineni et al. (1998) of an unforced plane wall jet using particle image velocimetry (PIV). For their experiment, the initial jet profile was parabolic, with an inflow Reynolds number of 800. They noted that the transition is dominated by the formation and development of discrete vortices in both the inner and outer regions.

Visbal et al. (1998) simulated an unsteady forced wall jet undergoing transition at a fixed Reynolds number of 2150, and compared it with a high resolution experimental measurements. The main parameters governing this incompressible wall jet were the inlet Reynolds number, the disturbance characteristics at the exit and the aspect ratio of the channel. The governing equations solved were the full unsteady two-dimensional incompressible Navier–Stokes equations supplemented by the perfect gas law, Sutherland's viscosity formula, and the assumption of constant Prandtl number (0.72). This numerical technique which avoids empirical modeling for the unsteady fluctuations is referred to as 2-D direct numerical simulations (DNS) and has been used by other researchers for similar flows, e.g. backward facing steps (Kim and Moin, 1985; Kaiktsis et al., 1991; Le et al., 1997).

It should be noted that a 2-D DNS technique simply reverts to a steady-state solution for laminar flows without span-wise geometry variations, while a 3-D DNS technique is appropriate for turbulent flows. For transitional flows which are just above the laminar regime and exhibit some unsteadiness, the primary instabilities and flow structures can be two-dimensional (e.g. the Karman vortex street behind a circular cylinder at Reynolds numbers of 100–200) and as such modeled approximately with 2-D DNS. However, care must be taken when interpreting such results, as three-dimensional features can quickly become critical features of the turbulent transition process.

Thus based on the previous experimental and numerical studies of laminar and early transitional wall jets, it is generally known that unsteadiness begins at about Re of 800 and the flow develops strong (though primarily two-dimensional) Kelvin–Helmholtz type vortices when excited at Re of 2000. What is not known, is the variation of the momentum entrainment as a function of Reynolds number for wall jets as the flow transitions from laminar conditions to the early transitional state. In addition, there have been no experimental or numerical studies which have investigated the influence of the initial jet velocity profile. Finally, there has been no detailed assessment of the viability of RANS type simulations in predicting the overall entrainment of the wall jet at moderate Reynolds numbers.

1.3. Study objectives and test conditions

The primary objective of this study was to increase the understanding of the effects of Reynolds number and velocity profile on the temperature distribution and time-averaged jet thicknesses of idealized refrigerated wall jets. To investigate the effects of the initial velocity distribution, three profiles were tested: parabolic (as found in laminar flow through parallel plates), uniform (i.e. plug flow at the exit) and a ramp profile (where the maximum velocity is at the wall and a constant linear decrease in velocity occurs until the outside edge of the jet is moving at the same speed as the co-flow velocity). Various stream-wise variations of $x/H = 10$, 15 and 20 are primarily considered as they correspond to typical air curtain lengths for display cases.

The Reynolds numbers at which the DNS approach is conducted (ranging from 100 to 2000) are in the laminar and early transitional range. For sufficiently low Reynolds numbers, a steady laminar solution will occur since no instabilities develop and a two-dimensional description is appropriate. For the early transitional conditions, the flows are primarily governed by stream-wise and transverse characteristics so that a two-dimensional approach may be employed. To assess the accuracy of the 2-D description at the highest wall jet Reynolds number of 2000 (where the difference is the most profound), comparison with results from 3-D DNS. At higher Reynolds numbers (up to 10,000), the RANS approach is used; however simulation at the Reynolds number case of 2000 will also allow direct assessment of this approach with the more computationally intensive DNS approach.

2. Methodology

2.1. Code description

The code employed in the present study is "WIND", which can provide time-accurate viscous 2-D and 3-D simulations of using a structured, multi-zone, computational approach (Bush et al., 1998). The gas is assumed to be calorically perfect and viscosity is obtained from the Sutherland viscosity law. The discretization of the equations of motion used in this study is set as a second-order (in space) physical Roe upwind with modifications for a stretched grid. It should be noted that the accuracy does not increase significantly by increasing the spatial discretization order from second to third. A global Newton time integration scheme was used (Tramel and Nichols, 1997), which solves the unsteady equations by placing them on the right-hand side of the matrix solver, and iterating within a time-step over all the zones. Thus, the interface boundaries are brought up to the new time level, along with the interior flow field, resulting in an essentially implicit treatment of the boundaries.

WIND allows for both a RANS approach (with turbulence modeling) as well as direct simulation of the full Navier–Stokes equations (no turbulence modeling). The flowfield of a wall jet involves both free shear and boundary layer features, the shear stress transport (SST) model was used for the RANS simulations in this study. The SST is a hybrid of two successful two equation models: the κ–ε and κ–ω model and was first proposed by Menter (1994). In this hybrid model, a blending function is introduced, which is set to 1 near the free-stream (yielding the κ–ε model solution) and 0 near the wall (yielding the κ–ω model solution). Cazalbou et al. (1994) have shown an improved prediction of the flow-field at the free stream boundaries. In addition, Yoder et al. (1999) did a study of the "WIND" code performance using the Menter SST model and its near wall accuracy for flow over a turbulent flat plate. The model was shown to give accurate results of the boundary layer thickness. Consistent with such RANS validation studies, the value of the free-stream turbulent viscosity ν_t was set to 0.001 cm/s^2 for the present study. For the laminar flow and DNS flow cases, a zero turbulent viscosity was employed. For these cases, the code was first validated for a canonical well-studied flow with laminar and early transitional conditions, the isothermal flow over a backward facing step was simulated at Reynolds numbers of 100–1200. The validation details are in Appendix A.

2.2. Boundary conditions and grid for the wall jet

The domain of the entire flowfield for the 2-D cases was $[x_{\max}, y_{\max}] = [40H, 40H]$. The stream-wise boundary conditions include an adiabatic viscous surface along the wall, while the far (parallel) boundary is modeled as an inviscid wall. The inflow boundary has the velocity profile specified while the outflow is characterized with a first-order extrapolation condition for all the conservative quantities, i.e. the stream-wise derivative of these variables were set to be zero at the outflow plane. This boundary condition was found to give superior performance (as compared to conventional back pressure specification) with respect to outflow convection of vortices with reverse flow regions. Notably, it has been recently demonstrated by Hagstrom and Nordstrom (2003) that extrapolation conditions for subsonic flow gives a reasonably good estimation for outflow boundary conditions if implemented significantly far from the field of interest. In the present flow, the exit domain was at $x = 40H$ but quantitative results presented herein were restricted to $x \leqslant 20H$ to ensure a negligible impact of the outflow conditions on any statistics. Fig. 1a–c shows three inflow conditions used for the wall jet—parabolic, ramp, and uniform all over a width H. To allow comparison at equal jet mass flow conditions, the Reynolds number was based on the mean jet velocity averaged across the profile. To be consistent with the air entrained from above the air-curtain in most display cases, a small co-flow velocity of 6.6% of the mean jet velocity was specified across the rest of the inflow boundary, i.e. from $y = H$ to $40H$ at $x = 0$. The temperature of the ambient air was specified as 288 K and that of the jet as 273 K in order to allow visualization of the thermal and mass mixing, however gravity was set as 0 in order to avoid the additional complexity of buoyancy effects (to be examined in a companion study).

The values of $\Delta x/H$, $\Delta y/H$ and Δt^* $(t/(\Delta x/U))$ were obtained in a manner similar to that employed in the back-step validation, however the parameter which was monitored for grid and time-step independence was the jet thickness (δ) since there was no flow separation from the wall). The jet thickness, represents the momentum entrainment and is quantified as the distance from the wall where the stream-wise velocity equals one-fourth of the peak velocity for a given stream-wise location, i.e.

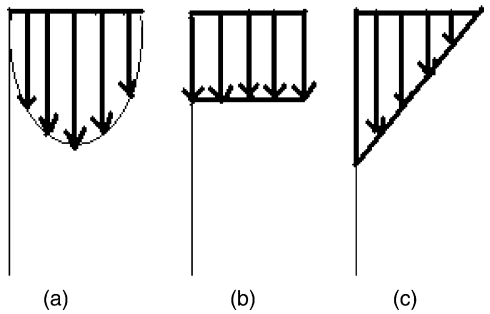

Fig. 1. Wall jet inflow profiles for: (a) parabolic, (b) uniform, and (c) ramp.

$u(x,\delta) = 0.25u_{\max}(x)$. A stretched grid corresponding to 65 grid lines across the initial jet profile height (H) was used to give a suitable grid resolution, corresponding to an average transverse spacing of $\Delta y/H = 0.0154$. This average spatial resolution was found to be sufficient with respect to jet thickness sensitivity (Fig. 2). A stream-wise grid study similarly yielded a grid spacing for the initial region ($\Delta x/H$) of 0.028 to be adequate. In terms of temporal resolution, a non-dimensional time-step $\Delta t^*(= \Delta t/V_{\text{jet}}H)$ of 0.025 was found to be similarly reasonable.

For the domain size sensitivity, different domain lengths in the x and y direction and many different domain configurations were tested. Various maximum domain lengths in the x-direction ($x_{\max}$) were tested including 20, 40, and $80H$, as was the case for $y_{\max}$. Both a $x_{\max}$ and a $y_{\max}$ of 40 were determined to ensure independence of the flow at $x/H < 20$ to the outflow conditions, while avoiding excess grid points. The final grid, shown in Fig. 3 is a clustered grid of 451×139, packed toward the flow inlet with uniform stream-wise resolution to $x/H = 12$, where H is the inlet height, after which it is stretched. In the y direction, the grid is clustered near the wall and expanded using a hyperbolic tangent function, the initial grid distance above the wall being $0.0008H$.

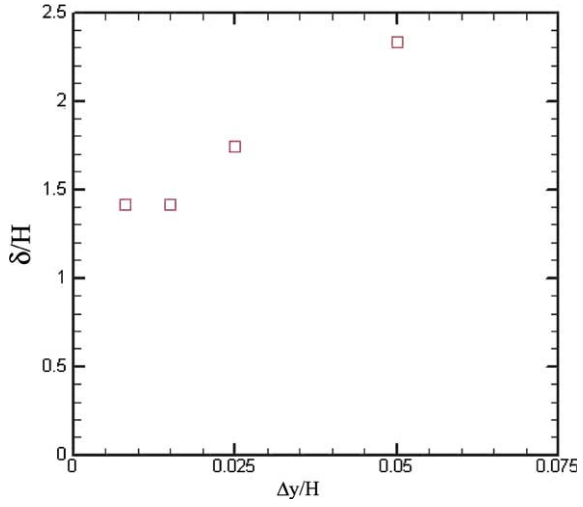

Fig. 2. Mean wall jet thickness vs. the traverse spatial resolution.

For the 3-D DNS approach, only the baseline test case ($Re = 2000$ parabolic inflow profile) was used for comparison to the 2-D results since it was the highest DNS Reynolds number and the most commonly investigated flow condition. For the 3-D case, a finite span-wise extent of $3.2H$ was introduced into the above 2-D wall-jet domain with periodic boundary conditions in the span-wise direction. where the distance in the Z direction is $3.2H$, with periodic wall boundaries were employed in the span-wise direction. This span-wise extent normalized by jet height was similar to that of Kaiktsis et al. (1991) for the back-step flow once normalized by channel height, which in turn was found to be sufficient to demonstrate the onset of three-dimensionality at large Reynolds numbers. The 3-D grid was simply an extension of the 2-D grid with a fixed number of span-wise planes. Based on span-wise grid resolution studies of the wall-jet of Visbal et al. (1998), a total of sixteen planes was deemed satisfactory ($\Delta z = 0.2H$).

The grid was then divided into 16 zones so that while running the code in parallel mode, each node can work on a one zone. The zones were divided to roughly contain the same number of grid points, and at least five grid points in either of the x, y or z directions. The solution was run for a t^* of about 140 to obtain time-averaged results on 16 processors. The total user time for this run on the NCSA SGI Origin 2000 was 4320 h, which corresponded to a wall clock time of about 320 h. For comparison, a single-processor run for a 2-D case

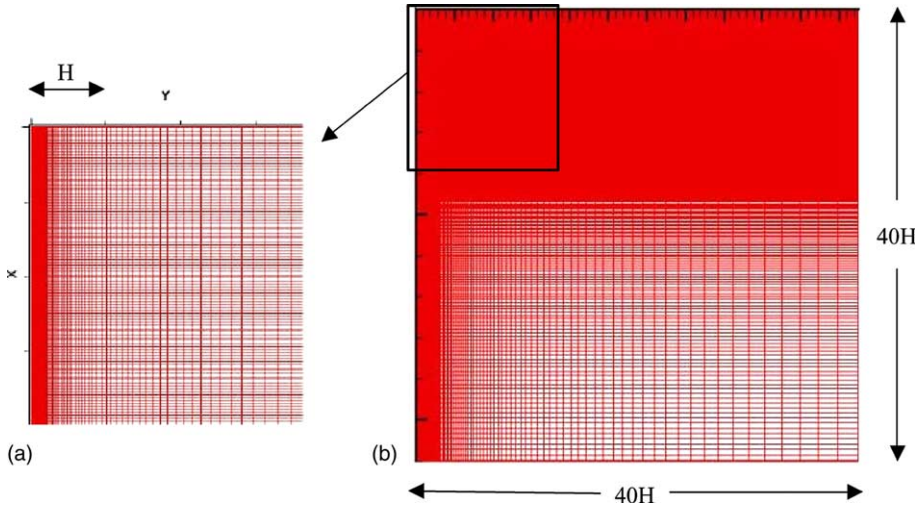

Fig. 3. Wall-jet grid showing: (a) close-up near inflow and (b) overall domain.

for a solution period of $140t^*$ took approximately 170 user hours. The RANS simulations required the least amount of CPU, e.g. typically 10 h on a single processor.

3. Wall-jet results

In the following section, computational results for the wall-jet (2-D DNS, 2-D RANS and 3-D DNS) are presented for a range of Reynolds numbers (100–10,000), x/H locations (10, 15, 20), and initial velocity profiles (ramp, uniform and parabolic) as specified in Table 1. The resulting velocity profiles were used to determine the flow dynamics and jet thickness (δ). Since the CPU usage of the 3-D DNS cases was nearly 20-fold larger as compared to the 2-D DNS cases, the majority of the simulations were conducted two-dimensionally in order to allow a comprehensive study and are discussed in the following. The RANS solutions were limited to two-dimensional flow only since the inflow conditions were two-dimensional and only steady-state solutions were employed.

3.1. Flow structures and dynamics

In the following, flow visualization of the numerical results was conducted to qualify the spatial and temporal structures for various flow conditions. Fig. 4 show the wall jet temperature contours at different Reynolds numbers from the laminar regime into the transitional/turbulent flow regime. The temperature contours are normalized by the ambient and jet temperatures such that $T^* = (T - T_{\text{jet}})/(T_{\text{ambient}} - T_{\text{jet}})$. In the range of $Re = 100$–700, the flow is laminar and the solution in steady. In general, the jet thickness tends to decrease as the Reynolds number increase as expected. In the range of Re from 700 to 2000, transitional effects are seen to cause a marked change in the Reynolds number effect. The flow at $Re = 700$ begins to show the production of eddies, and by $Re = 2000$, there is a regular production of eddies and the flow is clearly transitional. It is apparent that instabilities of the wall jet become more pronounced as the Reynolds number increases in this regime, yielding successively more pronounced Kelvin–Helmholtz type vortex structures (due to the shear flow instabilities). As a result, the jet tends to entrain by unsteadiness and become thicker as the Reynolds number increases. It is postulated here that the entrainment would always be least for the flow conditions when the flow just begins to change from the steady laminar regime into the early transitional regime, i.e. at about $Re = 700$. At the highest Reynolds number of 10,000, a RANS approach is used such that none of the unsteady flow structures are defined and a uniform diffusion is exhibited based on the empirically determined turbulent viscosity model. The mean flow development in this case is qualitatively similar to the $Re = 100$ case, indicating that the extreme Reynolds number conditions are likely to have the largest momentum entrainment.

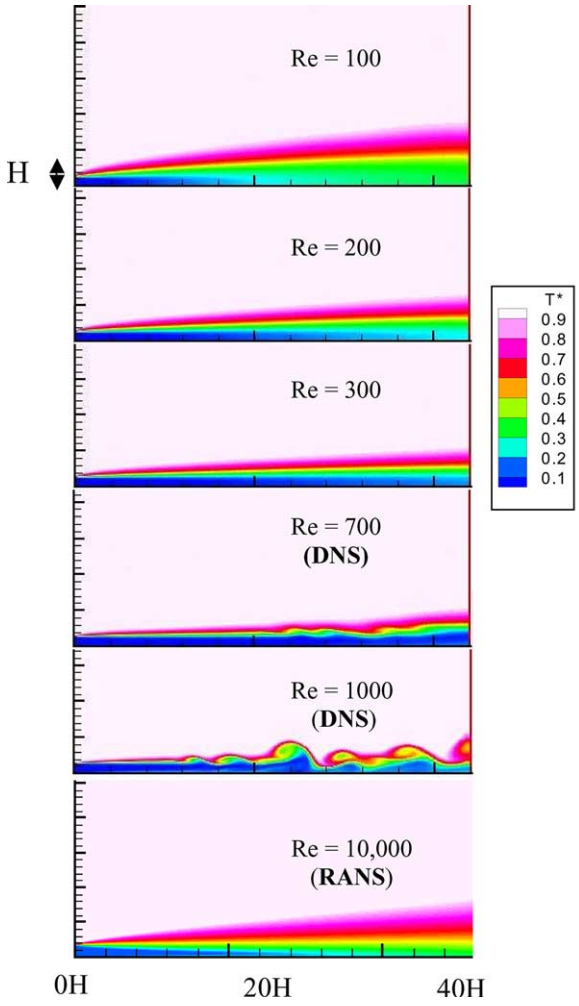

Fig. 4. Temperature contours at various Reynolds numbers for parabolic inflow profile.

Table 1
Investigated inflow test conditions

Inflow	DNS steady				DNS unsteady			RANS	
Parabolic	100	200	300	550	700	1000	2000	4000	10,000
Uniform	100	200	300	550	700	1000	2000	4000	10,000
Ramp	100	200	300	550	700	1000	2000	4000	10,000

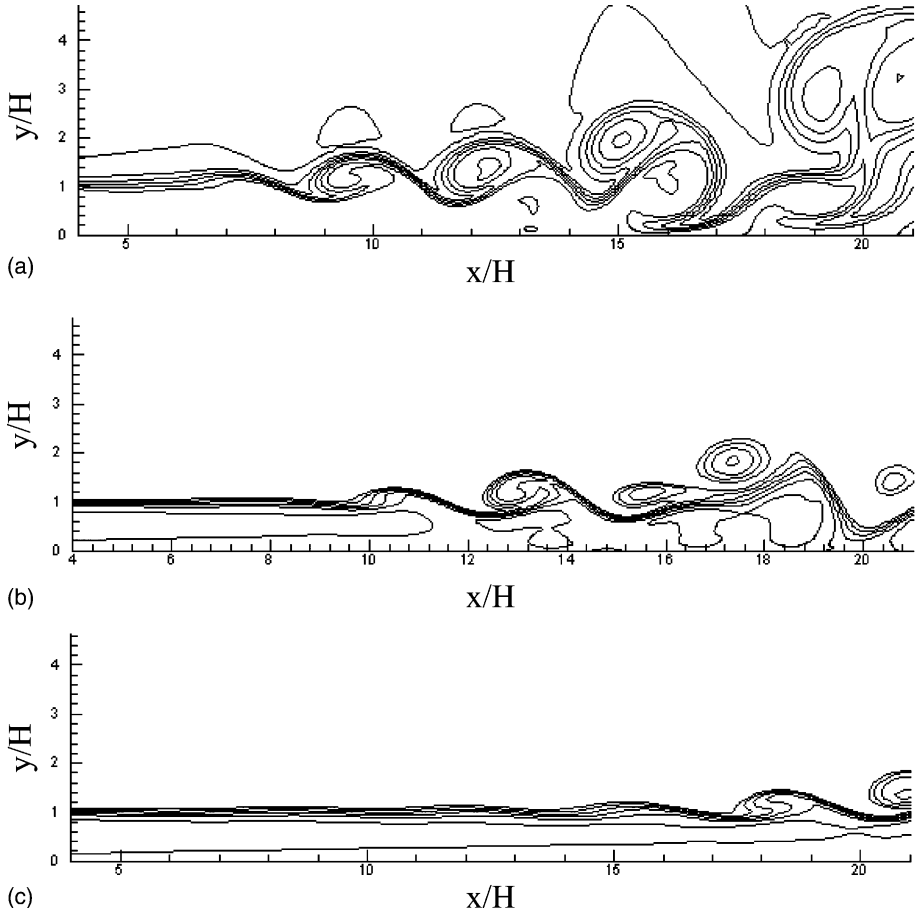

Fig. 5. Instantaneous temperature contour eddies at $Re = 2000$ for various jet flow profiles: (a) uniform, (b) parabolic, and (c) ramp.

Fig. 5a–c show the instantaneous flow visualization of the uniform, parabolic and ramp profiles at $Re = 2000$. The section of the flow shown is from x/H of 5 to 20. The onset of the initial eddy begins earliest in uniform profile case, and in turn occurs later for the parabolic and ramp profile cases. The rapid development of the uniform profile occurs because it has the steepest gradient amongst the three profiles and hence the local shear rates is higher such that instability and vortex formations begin faster. In the following, the vortex structures themselves are discussed.

In the case of the uniform and parabolic profile, the initial eddies appear to be of Kelvin–Helmholtz type, consistent with free-shear instabilities caused by the interface between the jet edge and the ambient flow. However, after which the eddies interact with the wall secondary mushroom type of vortices are formed downstream especially for the parabolic case. These structures have also been noted in forced wall-jet experiments (Visbal et al., 1998). It is also noted that the earlier onset of vortices tends to yield larger vortex sizes. In particular, in each case the initial eddy size is roughly $2.5H$, $2H$ and $1.5H$ respectively. Finally, the longer distance between in the ramp profiles indicates a less developed and unstable flow at this Reynolds number.

3.2. Wall jet thickness

The flow statistics for δ were obtained as a function of time for all cases at x/H of 10, 15 and 20. Fig. 6a–c shows the instantaneous momentum entrainment for $Re = 2000$, where each plot contains the parabolic, uniform and ramp profiles. These results indicate significant time-wise variations of the entrainment values. Notably the frequency, irregularity and amplitude of the variations increase with the increase in stream-wise distance. By the $x/H = 20$ distance, the uniform flow case it found to have the strongest variations and the largest thicknesses, while the ramp case yielded the weakest variations and the smallest overall thickness of the three profiles.

The velocity profiles were averaged over a large period of time, of order $100t^*$, which is sufficient to yield converged time-averaged values (note, the first $40t^*$ of the simulations were not averaged in order to avoid the initial transients). Fig. 7a–c show the time-averaged flow

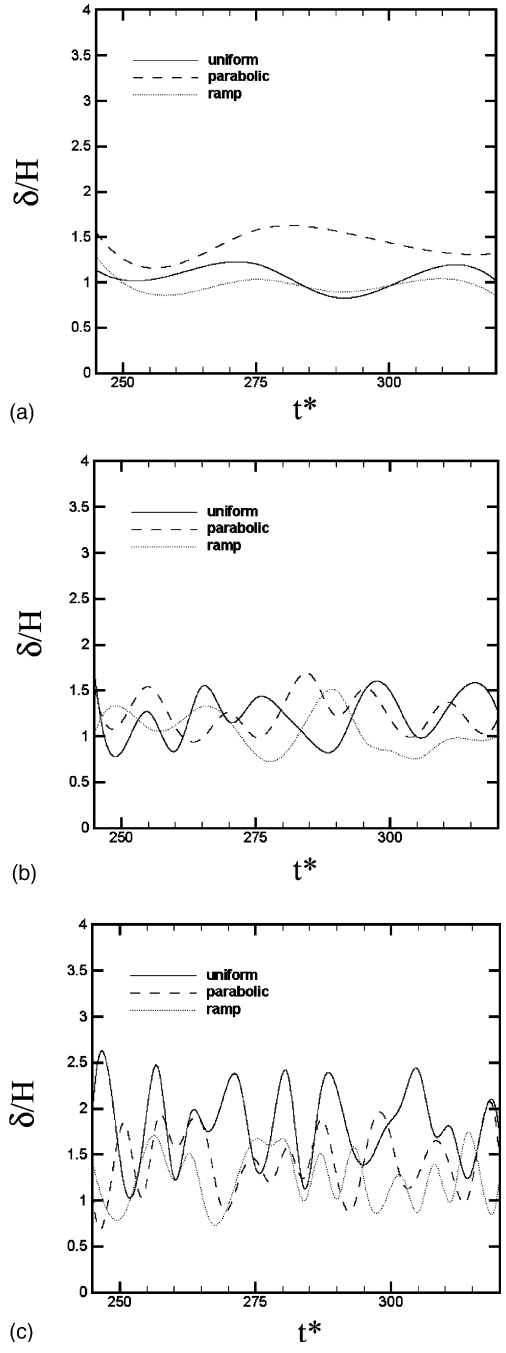

Fig. 6. Instantaneous wall jet thickness vs. time and $Re = 2000$ for various velocity profiles at: (a) $x/H = 10$, (b) $x/H = 15$, and (c) $x/H = 20$.

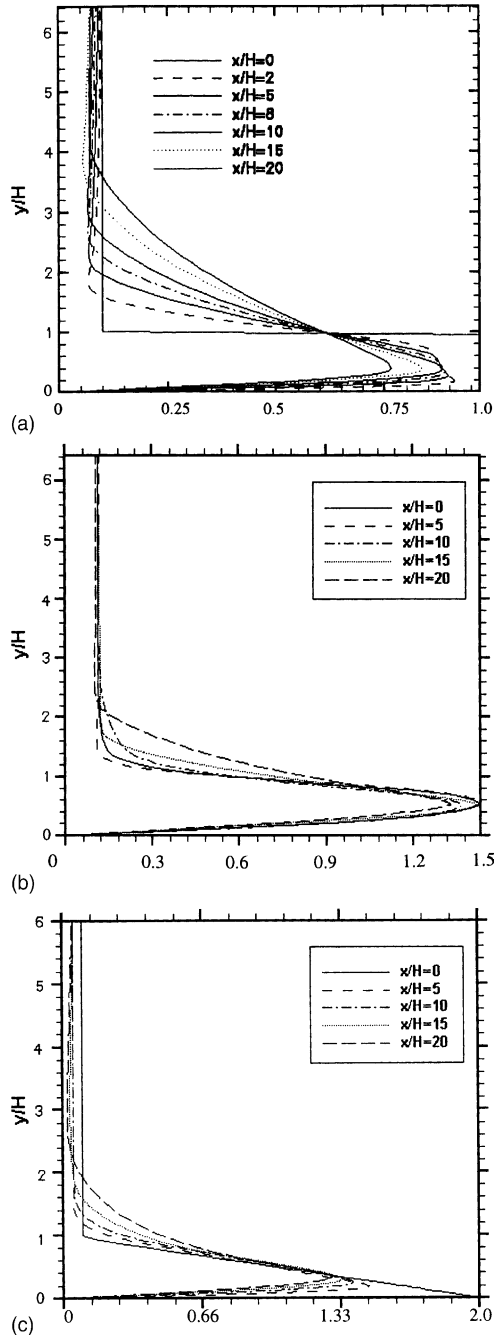

Fig. 7. Time-averaged velocity profiles at different stream-wise stations for $Re = 2000$ for the: (a) uniform, (b) parabolic, and (c) ramp inflow profiles.

profiles at different x/H stations normalized according to the U_{mean} of the uniform profile. In all cases, the velocity profiles become more diffuse as the develop downstream. However, there are distinct differences with respect to the degree of this diffusion and the near-wall variation. For the uniform initial velocity profile, the diffusion is rapid for transverse locations above $y/H = 1$. In addition, the peak stream-wise velocity reduces to about 75% of it's initial velocity with a successively increasing boundary layer thickness (defined as the distance from the wall to the velocity peak). For the parabolic velocity profile, the overall velocity shape remains approximately constant, especially near the wall, but above $y/H = 1$ the profile is seen to broaden. The ramp case is qualitatively similar to the parabolic case away from the wall, though the broadening is not so

fast. However, near the wall a boundary layer quickly develops and thickens to reduce the peak velocity, though it is still higher than the average mean jet flow velocity. Therefore, as the profile transitions from uniform, to parabolic to ramp profile, the peak stream-wise velocity tends to show successively greater retention of the mean jet velocity and lesser velocity broadening. Such characteristics are consistent with the instantaneous results, and indicate that the ramp profile is the least diffusive of the three cases, and can be expected to have the lowest ambient entrainment of the three cases (which is desirable for refrigerated display cases).

Fig. 8 shows the variation of the mean jet thickness with Reynolds number at the various stream-wise stations of the flow. In all of these plots the lower Reynolds number conditions (100–550) yield a flow in the laminar diffusion regime. This regime leads to a larger spread in the flow as viscous effects increase (i.e. as Reynolds number reduces), and hence larger wall jet thickness values as well. During the early transition period ($Re = 700$–2000) the entrainment sees a significant increase as the increased flow instabilities yield larger momentum mixing and thus jet thicknesses. However, at the higher Reynolds numbers (greater than 2000) where only RANS was employed the mean entrainment, as expected, only increased moderately from $Re = 2000$ to 10,000. The increased mixing predicted by the RANS approach is due to a continued increase in turbulent diffusion (and thus turbulent viscosity). As previously postulated, the jet thickness values were found to be least in the $Re = 700$–1000 range, i.e. when the flow just begins to change from the steady laminar regime into the early transitional regime. This result was found to occur for all velocity profile and at all stream-wise locations.

The influence of the inflow velocity profile also had an effect on the entrainment behavior, especially at higher Reynolds numbers where it can be as significant as the Reynolds number influence. In general, it was found that the ramp profile gave the consistently lowest entrainment, while the uniform profile gave the consistently highest entrainment. As such, the results indicate that the reduction of the local peak velocity gradients in the free-shear portion of the profile (the uniform flow contains a discontinuity at the edge which gives rise to a very high local gradient) generally yields a reduction in entrainment. This is because increased initial velocity gradients tend to germinate instabilities and thus vortices which in turn increases momentum and scalar diffusion rates (for laminar, transitional, and turbulent flow conditions). Conversely, the ramp profile minimizes the peak flow gradient and yields the lowest entrainment. Note, that the discontinuity in the wall region for the ramp profile did not significantly contribute to mixing, but this result may be different at higher Reynolds numbers than considered herein with the DNS approach.

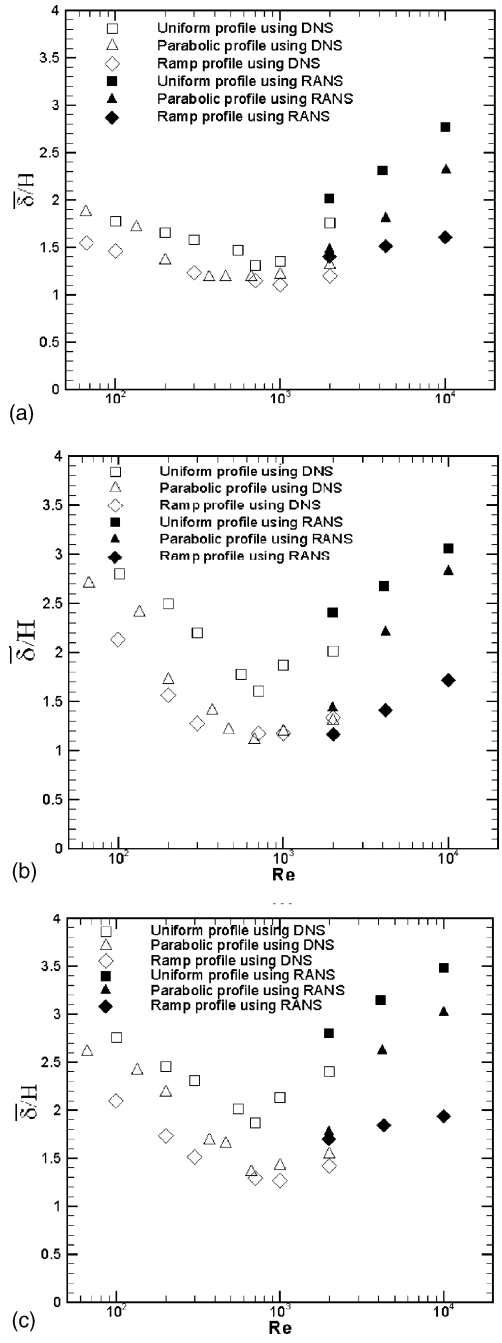

Fig. 8. Time-averaged wall jet thickness as a function of Reynolds number at a stream-wise station of: (a) $x/H = 10$, (b) $x/H = 15$, and (c) $x/H = 20$.

The jet thicknesses were also found to increase, as expected, with increasing stream-wise distance (x/H). However this effect was particularly strong for the laminar diffusion regime, compared to the transitional regime. This is because in the transitional case, the flow has already started generating vortices at an earlier stream-wise position after which the velocity does not change as rapidly (even though the thermal diffusion increases quickly), while in the laminar diffusion case there is no such "transition of the flow development.

Table 2
Comparison of time averaged momentum entrainment for 2-D DNS, 2-D RANS and 3-D DNS at $Re = 2000$ with parabolic inflow

Approach	At $x/H = 10$	At $x/H = 20$
2-D DNS	1.33	1.52
3-D DNS	1.36	1.53
2-D RANS	1.45	1.63

Lastly with respect to this figure, it is interesting to compare the DNS results (with no empiricism) and the RANS results (using the SST turbulence model) at $Re = 2000$. In general, it was found that the RANS consistently over-predicted momentum entrainment, especially for the uniform flow case at $x/H = 20$. This over-prediction is consistent with over-predictions by RANS studies in comparison to experiments of display-case air-curtains (Navaz et al., 2002; Baleo et al., 1995; George and Buttsworth, 2000). However, the discrepancies in values were rather moderate considering that the flows at these conditions are far from being fully-developed turbulence. The differences between the RANS and the 2-D DNS results are quantified in Table 2 for the parabolic condition. This suggests that RANS approach maybe at least qualitatively reasonable for the wall jet at Re of 2000 and higher, as long as large velocity discontinuities are not present.

3.3. Three-dimensional wall-jet

Fig. 9 shows a projection view of the 3-D wall jet case at $Re = 2000$ (the highest Reynolds number considered with the DNS approach). The 2-D rollers can be visualized for $X/H = 0$–20, after which the flow begins to show some 3-D (span-wise) variation in the temperature contours, though the structures remain largely two-dimensional. In order to more clearly see the three-dimensional influence, Fig. 10a–c show the velocity vectors superimposed upon temperature contours in the stream-wise and span-wise directions at various Y/H locations of $0.5H$, $0.75H$, and $1H$. Note that the velocity vectors are modified such that the span-wise component has been exaggerated by 10 times that of the stream-wise component in order to magnify the span-wise flow angularity (by about 10-fold). In general, the variation in temperatures appear primarily as 2-D disturbances up to about $X/H = 20$ (the regime for which the above results were reported) where the overall nature of the flow is quite similar to the 2-D results and supports the proposal that the flow features are mostly two-dimensional in nature. A similar conclusion was reached by Visbal et al. (1998) for a forced wall jet at $Re = 2150$ analyzed with both DNS and experiments. However, a striking feature of these figures is the significant correlation between high flow angularity (significant span-wise motion) and temperature fluctuations. Thus the primarily two-dimensional temperature perturbations arise simultaneously with the appearance of three-dimensionality of the velocity field, which may in turn play a substantial role in three-dimensionality of the thermal distribution. Further downstream ($X/H > 20$), the span-wise variations in the onset of temperature and velocity angularity are greater, especially as the flow is considered further from the wall, i.e. more 3-D effects are shown at $Y/H = 1.0$ than at $Y/H = 0.5$.

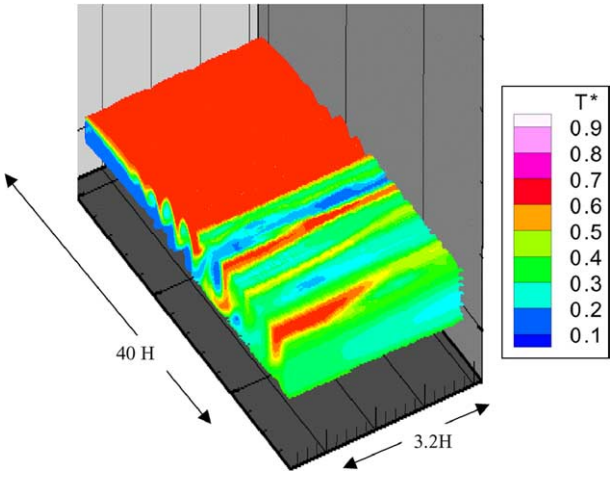

Fig. 9. The temperature contours of the 3-D wall jet visualized at a particular instant of time for $Re = 2000$ and parabolic inflow profile.

Fig. 11 show the instantaneous momentum entrainment (jet thickness) values from both the 2-D and the 3-D simulations for the same Reynolds number (2000) and inflow (parabolic), at stations $x/H = 10$ and 20. The frequencies of variation are very similar for both the 2-D and 3-D cases for both entrainments (though the 3-D variations is slightly more irregular). This irregularity becomes stronger at $x/H = 20$ when compared to the 2-D case, which is attributed to the onset of the three-dimensional effects at this more developed stream-wise location.

The time-averaged values of the entrainment were also obtained and compared, and given in Table 1, where it was found that the 2-D result tended to slightly under-predict the momentum entrainment with respect to the 3-D predictions, but that all the differences were less than 3%. The under-prediction by the 2-D approach, especially at higher x/H values, is consistent with additional mixing caused by the downstream development of some stream-wise vorticity effects as seen in Figs. 9 and 10. However, since the differences were, in general, minor, this indicates that the current 2-D results for Re of 2000 or less should be reasonably representative their 3-D counterparts. This is consistent with minor differences between the 2-D and 3-D DNS results for the backward facing step at early transitional Reynolds numbers (10) and the agreement between experiment and simulation for the exited wall jet of Visbal et al. (1998). Again, the RANS results are not

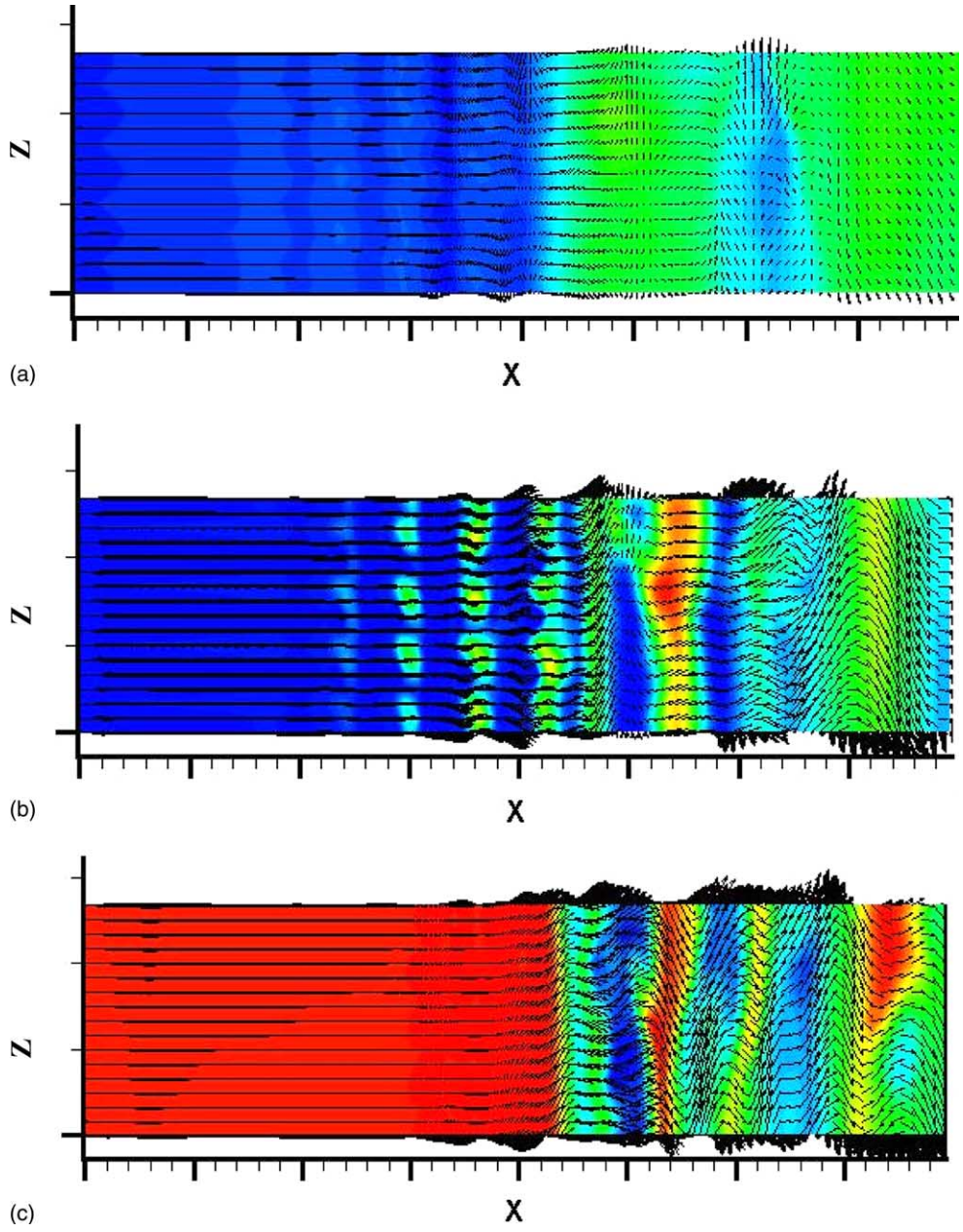

Fig. 10. Temperature contours and velocity vectors (exaggerated in the z direction 10 times) over the domain of $x/H = 0$–40 for: (a) $y = 1/2H$, (b) $y = 3/4H$, and (c) $y = H$ (see Fig. 9 for temperature legend).

much different than the DNS predictions (within 10%), which was a better than expected performance for this time-averaged numerical technique.

4. Conclusions

The variation of the thermal entrainment in a thermal wall jet was numerically investigated and it's variation with numerous flow parameters was investigated. Entrainment was found to increase in the stream-wise direction, especially for the lower (laminar) Reynolds numbers. It was also found that the jet thickness reached a minima at around $Re \sim 700$ corresponding to the point when the flow starts generating instabilities. This supported the hypothesis that the mixing levels would monotonically reduce as the Reynolds number increased up to the point where transition started, whereby increases in Reynolds number yielded substantial increases in mixing (in terms of both the momentum and the temperature distributions).

Various initial jet velocity flow profiles were also investigated and the ramp profile was seen to yield the least entrainment, whereas the uniform inflow profile

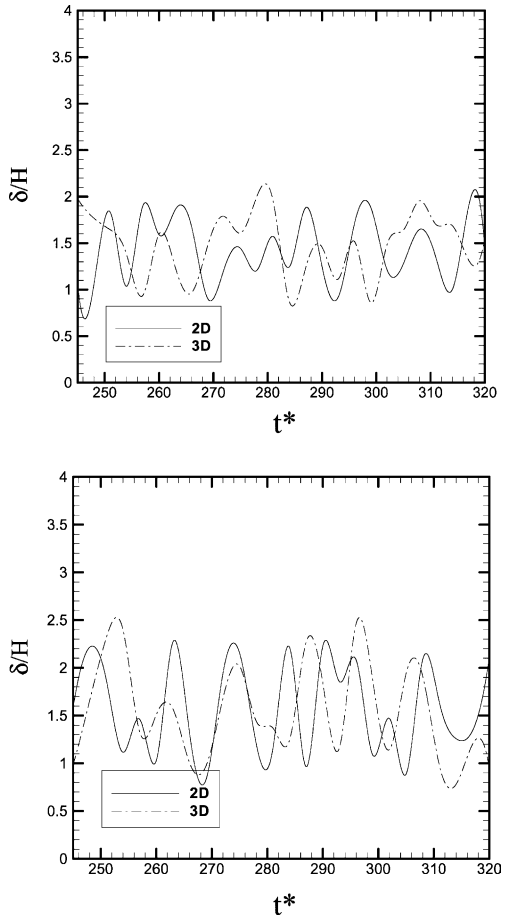

Fig. 11. Instantaneous wall jet thickness at $x/H = 10$ and 20.

yielded the highest entrainment. This trend was consistent with the hypothesis that the sharp discontinuity of the uniform step velocity profile (which yields a very high local velocity gradient just downstream) would result in increased mixing as compared to the ramp velocity profile (which had a more gradual velocity variation). Finally, a three-dimensional comparison study was completed, and the flow was found to be largely two-dimensional (but with some regions of significant flow angularity) up to a Reynolds number of 2000 for $x/H < 20$. However, at x/H of 20 or more yielded substantial three-dimensional effects, and were particularly strong in the transverse direction away from the wall at $y/H = 0.75$ onwards.

Acknowledgements

This study was funded by the Air Conditioning and Refrigeration Center at the University of Illinois at Urbana-Champaign (UIUC), and the simulations were completed using the resources of the National Center for Supercomputing Applications (NCSA).

Appendix A. Validation for the backward facing step flow

To assess the 2-D DNS approach, flow over a backward facing step at laminar and early transitional conditions was chosen for simulation. This flow has similar fundamental features as the wall jet, i.e. free shear flows and wall boundary layers combined, as well as published experimental and computational data for comparison. In particular, results were obtained by Oswald et al. (1983), while Le et al. (1997) conducted 3-D DNS investigations, and Kaiktsis et al. (1991) employed both 2-D and 3-D DNS simulations. The latter study found that the 3-D prediction of the separation extent was within 16% of that obtained from the 2-D result for a back-step Reynolds number of 1200. Thus, the backward facing step is well suited to allow the establishment of the present DNS methodology in terms of its predictive capability and typical spatial discretization requirements for laminar and early transitional conditions.

A parabolic inflow profile at the inlet (consistent with a fully developed laminar channel flow) was used for the backward facing step along with an outflow condition at the exit based on extrapolated pressure conditions. All walls were treated as viscous no-slip boundaries. The channel dimensions are such that the inflow comes from a unit step height from the point of expansion and the outflow is 40 step heights downstream. The two-dimensional grid was clustered near the side-walls of the back-step.

The re-circulation zone identified by the re-circulation length x_{sep} shown in Fig. 12, is generally noted to be a sensitive indicator of the flow features and therefore is well suited for evaluating spatial and temporal discretization convergence. A sample of the detailed grid sensitivity tests performed for this flow is given in Fig. 13 where the re-circulation length at $Re = 800$ was found to

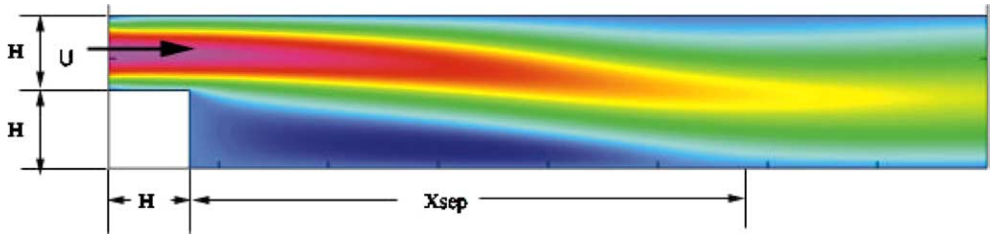

Fig. 12. Schematic of flow domain and stream-wise velocity contours at $Re = 300$ for the backward facing step.

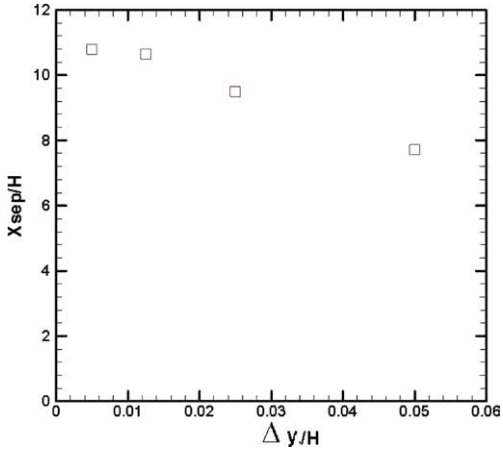

Fig. 13. Transverse grid spacing sensitivity at $Re = 800$ for backward facing step.

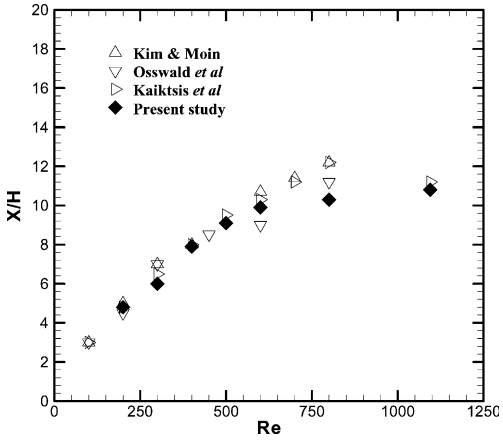

Fig. 14. Separation length as a function of Reynolds number for the backward facing step for various two-dimensional DNS predictions.

be grid independent for $\Delta y/H$ of 0.0125 or less, in addition spatial and temporal independence was also noted for $\Delta x/H < 0.0125$ and $\Delta t^* < 0.025$. Given these conditions, the re-circulation length normalized by the step height (x_{sep}/H) was obtained as a function of the Reynolds number and compared to previous experimental and computational studies in Fig. 14. For Reynolds number less than 600 the flow is nominally a steady laminar flow, at about 800 it begins to transition, although there is significant debate about the exact Reynolds number (Oswald et al., 1983). As a result, the flow reattachment length can be somewhat sensitive to minor differences in inflow conditions and numerical techniques. As such there tends to be a spread in the results at this condition and the present results are within such a variation. At the higher Reynolds number of 1095, the flow is definitely unsteady and the agreement with the available numerical results of Kaiktsis et al. (1991) is excellent. The good comparison for both laminar and early transitional regimes supports the present DNS approach for these types of flows.

References

Baleo, J.N., Guyonnaud, L., Solliec, C., 1995. Numerical simulation of air flow distribution in a refrigerated display case curtain. In: National Congress of Refrigeration Proceedings.

Bush, R.H., Power, G.D., Towne, C.E., 1998. Wind: the production flow solver for the nparc alliance. AIAA-98-0935.

Cazalbou, J.B., Spalart, P.R., Bradshaw, P., 1994. On the behavior of two-equation models at the edge of a turbulent region. Physics of Fluids 6, 1797–1804.

Field, B., 2001. Measurements of air curtain entrainment. Master's thesis, University of Illinois Urbana Champaign, December.

Field, B., Loth, E., 2001. Measurements of air curtain entrainment. In: Proceedings of ASME FEDSM 2001, May.

George, B., Buttsworth, D.R., 2000. Investigation of an open refrigeration cabinet using computational simulations with supporting equipments. In: IMECE, Orlando, FL.

Glauert, M.B., 1956. The wall jet. Journal of Fluid Mechanics 1, 625–643.

Gogineni, S., Visbal, M., Shih, C., 1998. Phase-resolved PIV measurements in a transitional plane wall jet: a numerical study. Experiments in Fluids 27, 126–136.

Hagstrom, T., Nordstrom, J., 2003. Analysis of extrapolation boundary conditions for the linearized Euler equations. Applied Numerical Mathematics 44, 95–108.

Hsiao, F.B., Sheu, S.S., 1996. Experimental studies on flow transition of a plane wall jet. Aeronautical Journal 100, 373–380.

Kaiktsis, A., Karniadakis, L.G.E., Orszag, S.A., 1991. Onset of three-dimensionality, equilibria, and early transition in flow over a backward-facing step. Journal of Fluid Mechanics 231, 501–528.

Kim, J., Moin, P., 1985. Applications of a fractional step method to incompressible Navier–Stokes equations. Journal of Computational Physics 59, 308–323.

Le, H., Moin, P., Kim, J., 1997. Direct numerical simulation of turbulent flow over a backward facing step. Journal of Fluid Mechanics 330, 349–374.

Menter, F., 1994. Two-equation eddy viscosity turbulence models for engineering applications. AIAA Journal 32, 1598–1605.

Navaz, H.K., Faramarzi, R., Gharib, M., Dabiri, D., Modarress, D., 2002. The application of advanced methods in analyzing the performance of the air curtain in a refrigerated display case. ASME Journal of Fluids Engineering 124, 756–764.

Oswald, G.A., Ghia, K.N., Ghia, U., 1983. Study of incompressible separated flow using implicit time-dependent technique. In: AIAA Sixth CFD Conference, Danvers, MA, pp. 686–692.

Tramel, R.W., Nichols, R.H., 1997. A highly-efficient numerical method for overset-mesh moving-body problems. AIAA Paper 97-2040.

Visbal, M., Gaitonde, D., Gogineni, S., 1998. Direct numerical simulation of a forced transitional plane wall jet. In: 29th AIAA Fluid Dynamics Conference, Albuquerque, NM, June (AIAA 98-2643).

Yoder, D.A., Georgiadis, N., Nicholas, J., 1999. implementation and validation of the Chien k–epsilon turbulence model in the WIND Navier–Stokes code. AIAA Paper 99-0745, January.